AD-A189 979 BEAM ASSISTED FABRICATION OF III-V/SI MONOLITHIC DEVICES(U) COLORADO STATE UNIV FORT COLLINS G Y ROBINSON 10 SEP 87 F49620-86-K-0021 1/1

UNCLASSIFIED F/G 9/1 NL

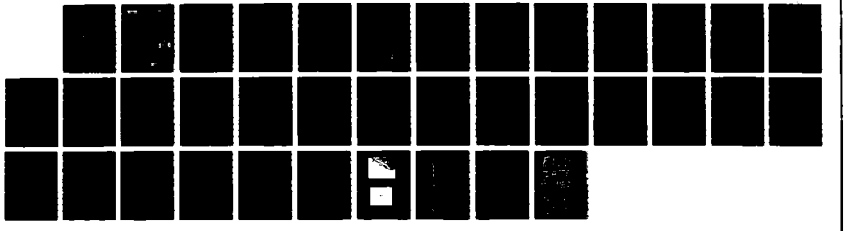

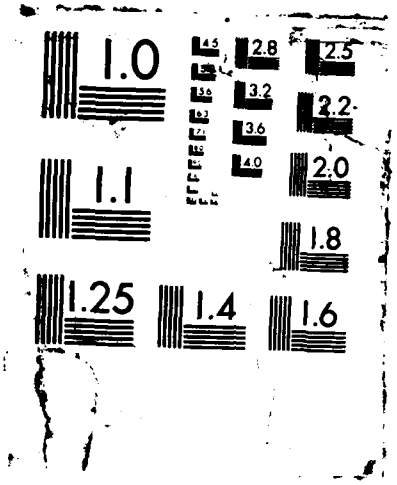
1.0
1.1
1.25
1.4
1.6
1.8
2.0
2.2
2.5
2.8
3.2
3.6
4.0
4.5

SECURITY CLASSIFICATION OF THIS PAGE

REPORT DOCUMENTATION PAGE

Form Approved OMB No. 0704-0188

AD-A189 979

1a. REPORT SECURITY CLASSIFICATION: UNCLASSIFIED

1b. RESTRICTIVE MARKINGS: DTIC FILE COPY

2a. SECURITY CLASSIFICATION AUTHORITY

2b. DECLASSIFICATION / DOWNGRADING SCHEDULE

3. DISTRIBUTION / AVAILABILITY OF REPORT
Approved for public release, distribution unlimited

4. PERFORMING ORGANIZATION REPORT NUMBER(S)

5. MONITORING ORGANIZATION REPORT NUMBER(S)
AFOSR-TR- 87-1888

6a. NAME OF PERFORMING ORGANIZATION: Colorado State University

6b. OFFICE SYMBOL (If applicable)

7a. NAME OF MONITORING ORGANIZATION: AFOSR/NE

6c. ADDRESS (City, State, and ZIP Code): Fort Collins, CO 80523

7b. ADDRESS (City, State, and ZIP Code): Bldg 410, Bolling AFB, DC 20332-6448

8a. NAME OF FUNDING / SPONSORING ORGANIZATION: AFOSR

8b. OFFICE SYMBOL (If applicable): NE

9. PROCUREMENT INSTRUMENT IDENTIFICATION NUMBER: F49620-86-K-0021

8c. ADDRESS (City, State, and ZIP Code): Bldg 410, Bolling AFB, DC 20332-6448

10. SOURCE OF FUNDING NUMBERS

PROGRAM ELEMENT NO.	PROJECT NO.	TASK NO.	WORK UNIT ACCESSION NO.
61102F	5548 DARPA	00	

11. TITLE (Include Security Classification): Beam Assisted Fabrication of III-V/Si Monolithic Devices

12. PERSONAL AUTHOR(S): Prof Robinson

13a. TYPE OF REPORT	13b. TIME COVERED	14. DATE OF REPORT (Year, Month, Day)	15. PAGE COUNT
Annual	FROM 09Nov86 TO 090ct87		

16. SUPPLEMENTARY NOTATION

DTIC ELECTE JAN 14 1988 S D H

17. COSATI CODES			18. SUBJECT TERMS (Continue on reverse if necessary and identify by block number)
FIELD	GROUP	SUB-GROUP	SILICON

19. ABSTRACT (Continue on reverse if necessary and identify by block number)

The objective of this research project is to explore two new methods for deposition of III-V semiconducting films on Si substrates. Using gas-source molecular beam epitaxy (MBE) and photon-beam and electron-beam assisted metal-organic chemical vapor deposition (MOCVD), GaAs and other III-V films with abrupt heterojunctions are being formed epitaxially on Si, and by means of optical and electrical characterization the suitability of the resulting III-V/Si structures are being examined for use in monolithic devices.

ARCODE

20. DISTRIBUTION / AVAILABILITY OF ABSTRACT
☐ UNCLASSIFIED/UNLIMITED ☐ SAME AS RPT ☐ DTIC USERS

21. ABSTRACT SECURITY CLASSIFICATION: UNCLASSIFIED

22a. NAME OF RESPONSIBLE INDIVIDUAL	22b TELEPHONE (Include Area Code)	22c. OFFICE SYMBOL
Malloy	(202) 767-4931	NE

DD Form 1473, JUN 86 — Previous editions are obsolete. — SECURITY CLASSIFICATION OF THIS PAGE

Annual Report

First Year
(9/11/86 - 9/10/87)

"Beam Assisted Fabrication of III-V/Si Monolithic Devices"

AFOSR Contract #F49620-86-K-0021

Colorado State University
Fort Collins, CO 80523

PI: Gary Y. Robinson

Co PI's: George J. Collins
Raj Solanki (Oregon Graduate Center)

Annual Report
(Covering 9/11/86 - 9/10/87)

"Beam Assisted Fabrication of III-V/Si Monolithic Devices"

The objective of this research project is to explore two new methods for deposition of III-V semiconducting films on Si substrates. Using gas-source molecular beam epitaxy (MBE) and photon-beam and electron-beam assisted metal-organic chemical vapor deposition (MOCVD), GaAs and other III-V films with abrupt heterojunctions are being formed epitaxially on Si, and by means of optical and electrical characterization the suitability of the resulting III-V/Si structures are being examined for use in monolithic devices.

Gas-Source MBE (Gary Y. Robinson, Colorado State University)

Gas-source MBE combines thermal cracking of the gaseous hydrides AsH_3 and PH_3 to produce molecular beams of As_2 and P_2, respectively, with conventional MBE technology for Group-III molecular beam production from effusion cells. The availability of both As_2 and P_2 beams allows incorporation of buffer layers of wide composition range and lattice parameters and for exploration of III-V materials grown by MBE on Si other than GaAs.

The major accomplishments of the first year consisted mainly of design, procurement, installation, and check-out of the custom equipment needed for gas-source MBE. The major equipment items were (refer to Figures 1 and 2):

- Gas delivery system for the hydrides with provision for precise control and rapid switching of PH_3 and AsH_3 flow rates. We designed the system, it was built to our specifications by a commercial vendor, installed, and checked out in our laboratory.

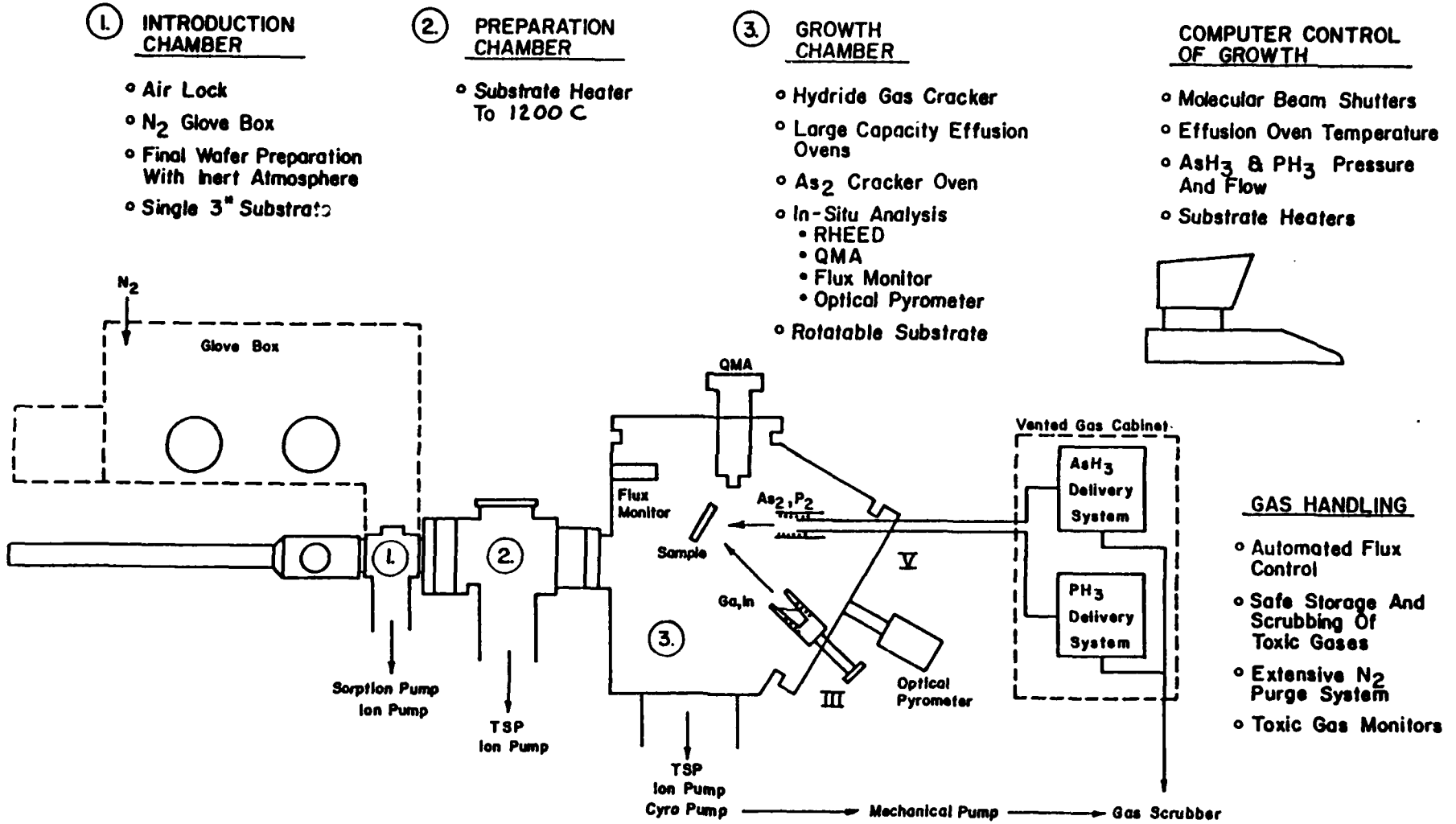

FIGURE 1 **SCHEMATIC DIAGRAM**

MOLECULAR BEAM EPITAXY SYSTEM

COLORADO STATE UNIVERSITY

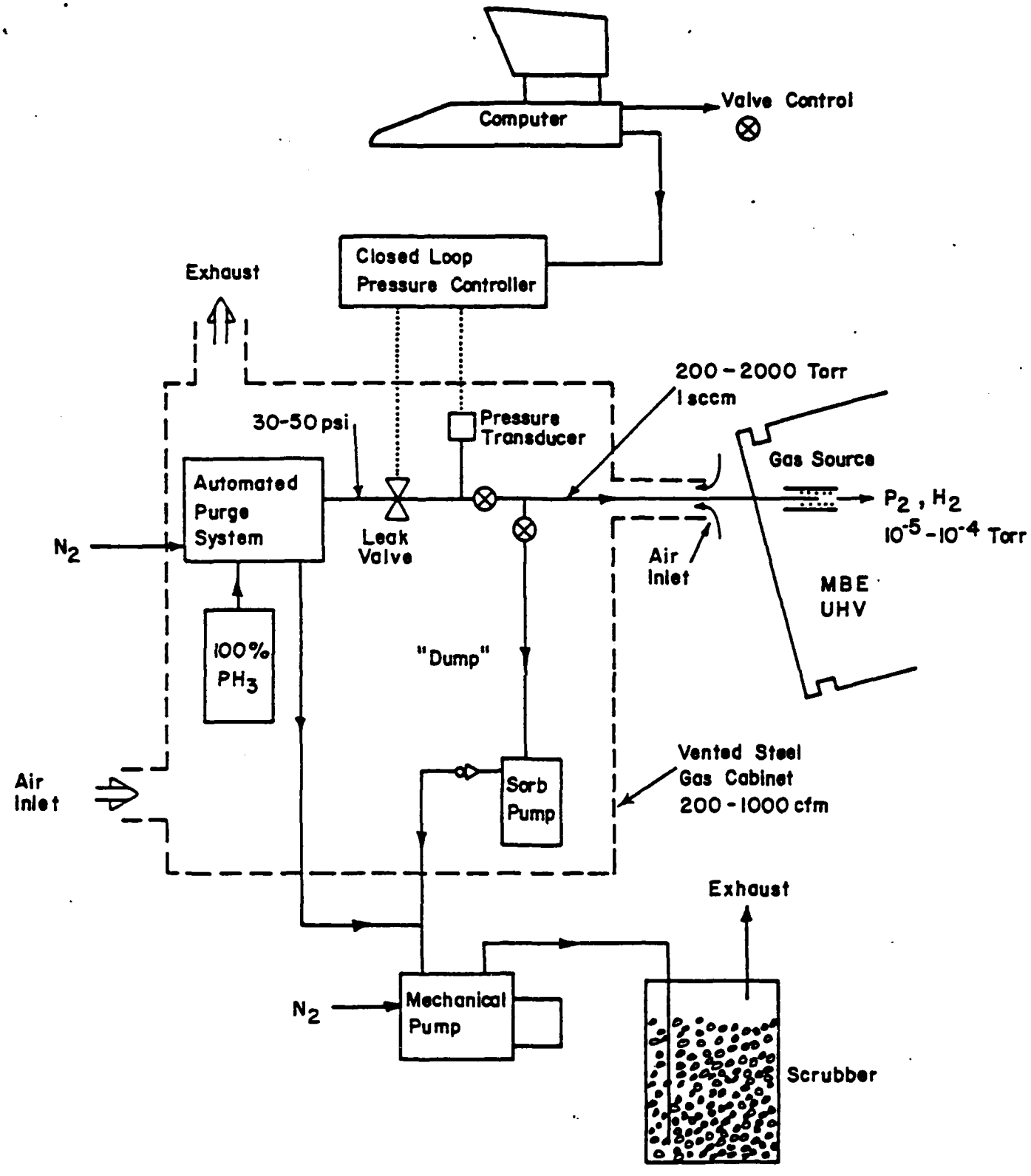

FIGURE 2 **SCHEMATIC DIAGRAM**

HYDRIDE DELIVERY SYSTEM

- Gas-cracking oven for reducing the hydrides PH_3 and AsH_3 to molecular beams of P_2 and As_2. After design by us, a cracking oven was built in Japan and delivered late in the year.

- Pumping system to accomodate the large H_2 gas load and for safe removal of the toxic hydrides. The system consists of a He closed-cycle cryopump, mechanical pump, and gas scrubber.

- Other specialized equipment needed for growth and characterization of films on Si substrates. These included:
  - Glove box for MBE introduction chamber for preparation of Si wafers in oxygen free atmosphere,
  - New substrate heater for cleaning Si at temperatures as high as 1200C, and,
  - A double-crystal X-ray diffractometer for structural characterization of III-V films on Si.

All of the above equipment is now in place and is being integrated into one system with a single computer for control of the MBE growth process.

While the above equipment was being put into place to provide gas-source MBE capability, epitaxial growth using conventional MBE was undertaken. During the first year we have grown:

- GaAs on Si to establish the proper Si substrate cleaning techniques and growth procedures in our laboratory,

- InGaAs/GaAs superlattices on GaAs. We intend to use superlattices of InGaAs/GaAs as a buffer layer to pin misfit dislocations when growing GaAs and other III-V layers on Si. X-ray diffraction spectra (see Fig. 3) indicate sharp heterojunction interfaces and excellent coherency of the periodic structure.

- GaAs on GaAs to qualify our new MBE system. Characterization included Hall-van der Pauw, C-V profiling, photoluminescence, SIMS, AES, and X-ray diffraction.

Efforts for the second year will exploit the specialized equipment installed and made operational during the first year by growing InP on Si using gas-source MBE. Buffer layers of GaAs and InGaP will be examined as well as direct grown on Si.

Figure 3

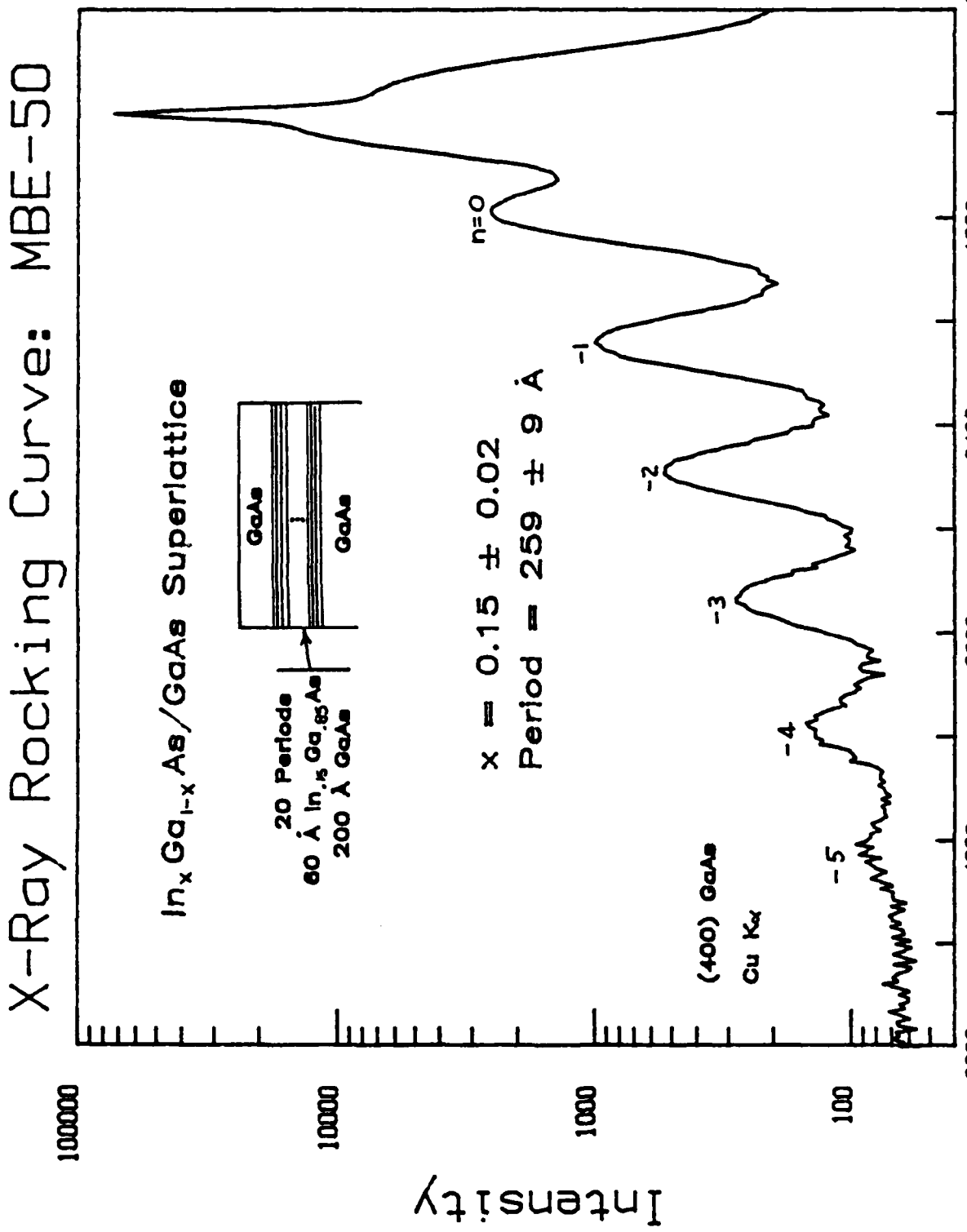
X-Ray Rocking Curve: MBE-50
$In_xGa_{1-x}As/GaAs$ Superlattice
20 Periods
60 Å $In_{.15}Ga_{.85}As$
200 Å GaAs
GaAs
GaAs
x = 0.15 ± 0.02
Period = 259 ± 9 Å
(400) GaAs
Cu K_α
n=0
-1
-2
-3
-4
-5
Intensity
100000
10000
1000
100
-6000
-4800
-3600
-2400
-1200
0
Angle (Arc Sec)

Energy Assisted Deposition of GaAs on Si (G. J. Collins, Colorado State University)

The progress of the growth of GaAs on Si with an energy assisted technique has been in the development of the deposition technique, realization of the reactor and support system design, and the completion of a proposal for further funding. The development of the deposition technique and the completion of the proposal has directed our research. The reactor design is a consequence of that effort. The laser assisted technique originally proposed has the advantage for both direct writing and low temperature deposition. However, the working with the laser can be problematic as well as the high cost may be prohibitive for the commercial development. As a result we have pursued the development of the electron beam for energy assisted deposition techniques. The realization of such an energy source has paralleled the GaAs on Si research. Organometallic feedstock gases have been decomposed and AlN films deposited and results presented in the attached preprint (Appendix A). This deposition technique is very relevant and is being applied to our GaAs on Si research since it possesses many advantages in both the gas phase decomposition of the gases as well as the composition of the deposited films.

The proposal has just been completed and represents our efforts to elucidate the physical problems associated with the III-V deposition on Si and our proposed solutions. Funding will be sought as the proposal is being sent out in the middle of October.

Laser Induced Epitaxy of III-V Compounds (Raj Solanki, Subcontract to Oregon Graduate Center, Starting Date: December 1, 1986).

During the first year, most of our efforts were directed towards the construction of the laser deposition system. Although most of the construction was completed at the end of the second quarter, additional modifications were incorporated during the third quarter. At this time initial depositions were also achieved.

The process of laser-induced heteroepitaxy of III-V compounds is new and not well characterized, therefore we started with a simple system, i.e. growth of GaP on Si since they have a close lattice match. In order to systematically approach this issue, we spent the last quarter by first characterizing the homoepitaxy of GaP. This phase of our investigation provided us with a wealth of information on the laser process. Some of these results are summarized in the attached preprint (Appendix B). The empirical results obtained are used to help us develop a model of this growth process.

Over the past month, we have been investigating heteroepitaxy of GaP on Si. The deposition conditions here are significantly different than from homoepitaxy, however, we are making good progress. We expect to continue working on the heteroepitaxy of GaP on Si for the next few months before moving on to heteroepitaxy of other III-V compounds on Si.

Appendix A

LASER ENHANCED CVD OF ALUMINUM NITRIDE ON INDIUM PHOSPHIDE SUBSTRATES

T.Y. SHENG, L.R. THOMPSON, T. HWANG AND G.J. COLLINS

DEPARTMENT OF ELECTRICAL ENGINEERING

COLORADO STATE UNIVERSITY

FORT COLLINS, CO 80523

ABSTRACT

The chemical and electrical properties of laser CVD aluminum nitride deposited on n-InP substrates have been investigated. XPS and AES have been used to analyze the AlN-InP interface and the bulk chemical composition. FTIR was used to characterize water and OH bond content. The aluminum to nitrogen ratio of the laser deposited film is approximately 1, comparable to a conventional thermal MOCVD AlN film. Photoluminescence (PL) has been found to provide a convenient probe of surface sensitive properties of InP following wet chemical cleaning and AlN film deposition. The acidic solution clean of the n-InP wafers prior to film deposition gives rise to high PL intensity, whereas a basic solution gives rise to a low PL signal. PL measurements were correlated with the observed C-V characteristics of laser deposited AlN/InP MIS structures. A strong inversion layer can be formed in the n-InP substrate. The surface state density distribution has a minimum about 3×10^{11} $eV^{-1}cm^{-2}$ located 0.4 eV below the conduction band. Frequency dispersion of the AlN/InP MIS structures biased into accumulation is attributed to the bulk insulator while the frequency dispersion in the

depletion region is caused by the surface states at the insulator-semiconductor interface.

I. INTRODUCTION

Herein, we report low temperature laser CVD of AlN, outline deposition conditions, and present both chemical and electrical characteristics of laser deposited AlN/InP MIS structures. The interfacial characteristics of insulator/semiconductor structures on III-V compounds have been studied extensively in recent years( ). One dielectric type contains native oxides grown by using thermal or anodic techniques while a second type is a deposited insulator. One advantage of the native oxide growth is that surface contamination problems can be minimized since the process of oxidation results in the formation of a subsurface interface. However, the native III-V oxides are not satisfactory insulators primarily because the band gap of the III-V native oxides is smaller than that required for an acceptable dielectric insulator. With the deposited insulator, process induced surface damage to the III-V substrate often occurs giving rise to a large interface trap density. Moreover, conventional high temperature deposition processes are not suitable for III-V compound semiconductors due to incongruent thermal decomposition.

Aluminum nitride films are used in microelectronics, optical, and integrated optic applications( ) as a non-absorbing, non-dispersive high refractive index material( ). It has chemical, physical and electrical

properties suitable for these applications. The large bandgap of aluminum nitride (6 eV) makes it a very good insulator( ). Its low diffusion coefficients for impurities makes it a canidate passivating layer for semiconductor devices. Unlike most Al containing III-V compounds, aluminum nitride is stable in air as well as in vacuum to high temperature( ). Aluminum nitride also allows reduction of interface trap densities in InP MIS structures, provided there is an absence of oxygen during film deposition; hence, reduce native oxide growthoccurs at the interface. Finally, aluminum nitride is a III-V material, therefore, it is electrically inactive in a III-V compound semiconductor substrate such as InP and GaAs ( ). In other words, AlN-InP or AlN-GaAs interdiffusion, if there is any, is not expected to induce major detrimental effects.

Common to previously reported MIS structures on III-V substrates are two major problems: an undesired curreny drift and interfacial instabilities. The instabilities have been shown to depend on surface preparation and surface damage induced during insulator deposition. Our results presented herein suggest that laser assisted CVD may provide less radiation damage to the substrate surface as well as the use of a lower deposition temperature. This conclusion is supported by the measured properties of MIS structures given in part IV.

II. EXPERIMENT

A large number of process steps are involved in the fabrication of a simple metal-insulator-semiconductor(MIS) structure on InP and MIS electrical properties are effected by all combined process steps. In order

to better isolate the effects of each processing step, photoluminescence(PL) measurements can be used prior to and after each step of the MIS fabrication process( ), to monitor the changing electronic properties of the InP surface and acts as a guide to help determine the optimum processing sequence for making MIS diodes or MISFETs as shown below.

The n-InP substrates were first chemomechanically polished in a 1% bromine methanol solution. The wafers were then subjected to various chemical etches and PL measurements were carried out in air following each chemical cleaning sequence. InP samples were etched in the following active chemicals: (1) A single step etch in 4H SO : 1H O : 1H O; (2) A three steps etch including NRL (1HF : 1HCl : 4H O), 12 ml NRL with 1 drop H O and HCl(10%) and HF(10%); (3) A one step H O aqueous solution. Comparisons between the etches used were quantified by the observed PL data.

The experimental setup for the PL measurements is shown in Fig. 1. The front InP surface was illuminated with an He-Ne laser(= 633 nm) at a power density of 1 W/cm . An optical filter removes background light other than the 633nm radiation. The optical penetration depth for a 633nm photon impinging on an InP wafer is of the order of 150nm( ). The integrated PL signal is picked up from the back side of the InP sample and detected by a silicon photodiode. The observed PL intensity was distinct to each etch and correlated with C-V data as described in section IV.

A schematic diagram of the laser CVD system and typical deposition conditions are shown in Fig. 2 and Table I, respectively. The samples upon which AlN was to be deposited were first cleaned as described above, placed into a vacuum chamber and turbomolecular pumped for 2 hours. The base

pressure as monitored by an ion gauge was in the mid-of 10 Torr. During the pumping period, the samples were maintained at 150 C to assist desorption of water vapor and other surface contaminations. A Lumonics excimer laser operating on the 193nm ArF* transition was used to photo-dissociate the feedstock reactant gases chosen for the AlN deposition. Our choiced feedstock gases were trimethylaluminum (TMA: Al(CH)) and ammonia (NH) to obtain Al and N atoms respectively. Both TMA and NH absorb 193nm radiation strongly and form free radicals( ). Dissociated free radicals both react in the dissociation volume and condense on the substrate underneath the beam-dissociation region to form a film. We make no attempt in this work to unravel molecular gas phase kinetics nor competing surface reactions.

The macroscopic LCVD deposition parameters affecting AlN film properties were found empirically to include: the laser power, TMA/NH flow rate ratio, ambient background pressure of the CVD reactor and the choice of substrate temperature. During AlN film deposition, the substrate temperature was maintained at 300 C for the InP substrate, the highest temperature we can sustain without causing incongruent decomposition( ). Total reactor pressure was controlled by a downstream automatic butterfly valve and a mechanical pump. TMA/NH flow rate ratios were fixed at a value of 1:40 after prior empirical studies. The typical LCVD deposition rate is about 150 A/min. The refractive index and thickness of the AlN have been determined by an ellipsometer. Typical index value for the LCVD films are 1.70 to 2.0 (bulk value 2.18). It was noted that both the index and the electrical resistivity increase as the substrate temperature employed

increases. Simply speaking, using laser CVD, we deposit aluminum nitride films which have properties comparable to AlN films deposited by using conventional thermal CVD. Note that thermal CVD requires substrate temperatures greater than 800 C, which is not acceptable for InP substrates. AlN film properties for both thermal and laser techniques are compared in Table II.

After AlN deposition, post-deposition annealing occurs at 325 C, in Ar forming gas for 30 minutes. This anneal has been used to improve the semiconductor-insulator interface properties. Next a front contact to the MIS structure is formed by evaporating a pattern of circular aluminum dots on the AlN film approximately 5x10 cm in area and 1000A in thickness. Indium soldering on the InP backside was used to make ohmic contact to the n-InP substrate. The electrical properties of this MIS structure are giving in section IV.

III. XPS, AES AND FTIR STUDIES OF LCVD AlN THIN FILMS

Large variations in the MIS structures electrical properties were observed when the deposited insulator preparation procedure varied. This is judged due to changes in the interface native oxide. The undesired native oxide generates both fast interface states and provides bulk trapping sites. Therefore, we studied the structure of the interface oxide layer via XPS and AES in order to better understand the measured MIS electrical properties.

Atomic bonding and chemical composition of native oxide films grown on InP as a consequence of different chemical treatments were comparaed by the X-ray photoelectron spectroscopy (XPS) technique. XPS spectra were

obtained with a Perkin-Elmer Physical Electronics model 548 AES/ESCA system using a Magnesium X-ray target source. The rastered sputter gun used for XPS depth profiling operated at 1KV, 10 uA/cm current densities over 7x7 mm sample area. The XPS compositional profiles of InP wafer treated with 4H SO : 1H O : 1H O shows spectra that suggest the native oxide consists of InPO , although a small P-oxide signal is present. That is, the peak seperation between the P-InP and the P-oxide peak is approximately 4.5 eV, which corresponds to the value observed for InPO ( ). The seperation between the O 1S and the P-oxide peak is 398.2 eV also indicating that this P-oxide is bonded as InPO ( ). In addition, in curve fitting the In 3d line at the surface, two peaks were used and a good fit was obtained by holding the width of In-IrP (FWHM = 1.67 eV) peak constant. The seperation of the two peaks is 1.3 eV, which is in accordance with prior InPO work( ). The XPS compositional profiles of an InP wafer cleaned with H O were characterized by the thickness of the native oxide. It was much thicker for a H O clean as confirmed by ellipsometric thickness measurements. Our XPS data show that the composition of the native oxide with H O cleaning is also InPO . Other compounds such like In O , P O may be present in the InPO oxide layer, however, their presence is hard to quantitate due to the weak XPS signal of the P-oxide. The O 1s peak processes a 2.8 0.1 eV FWHM which indicates that H O cleaning creates InP samples which have thicker as well as multi-components oxides. Prior researchers( ) attribute to this native oxide the observations of both current drift and C-V hysteresis. Fig. 4 shows that the InP substrate etched by a H SO solution prior to AlN deposition has less hysteresis than a substrate treated with a H O cleaning

solution. Both the larger surface state density and observed C-V hysteresis of the sample with H O predeposition cleaning may be attributed to the existance of thicker native oxides.

The bulk composition of deposited films on InP substrates were also examined by Auger electron spectrascopy (AES). AES were obtained by using a Perkin-Elmer Physical Electronics model 548 AES/ESCA double pass CMA Auger spectrometer operating in dN/dE mode. Incident electron beam energy was 3 KeV with a typical beam current of 15 uA. Ion sputtering for depth profiling was performed with a beam of Ar ions. Reference samples of both Al O and AlN were available. Anodically grown Al O was used as a reference to identify the Al(KLL) and O(KLL) peak amplitudes in the Al O matrix. A MOCVD AlN film was used as a reference sample to identify the Al(KLL) and N(KLL) peak amplitudes in the AlN matrix. Relative atomic sensitivity factors (ASFs) of the O(KLL), Al(KLL) and N(KLL) characteristic peaks, as estimated from both anodically grown Al O and MOCVD AlN reference films, are 0.42, 0.055 and 0.25, respectively. The relative peak to peak intensities of O, Al and N spectra characteristic of LCVD AlN films were then measured and compared to the standards in order to determine the AlN film composition. The AES composition determination was verified by RBS analysis done at Sandia Laboratories. Both techniques give a 1:1 atomic ratio for AlN. The oxygen contamination varied from 5% when employing a 200 C substrate temperature to less than 1% for a 400 C substrate temperature.

Fourier transform infrared (FTIR) absorbance spectra of LCVD AlN samples were examined in the spectral range 4400 cm to 400 cm . The main

absorption peaks observed in the FTIR spectrum are discussed below. Peaks centered around 3450 cm and 1640 cm are related with impurity water bands ( ). These bands are significant for samples deposited at 200 C substrate temperature but decrease dramatically for samples deposited with increasing temperatures. The absorption band around 460 cm was observed for films deposited with low temperature but diminished when deposition temperature is higher than 300 C. This is consistent with the identification of the absorption peak at 460 cm to a vibrational mode of the Al O molecule( ). The spectrum shows peaks around 610 cm , 655 cm and 670 cm , which corresponds to lattice TO phonons in AlN( ). These three peaks exhibit increased intensity and sharpen in shape with increasing deposition temperature. These results support the AES analysis for oxygen contamination in LCVD deposited AlN films.

IV. MIS ELECTRICAL MEASUREMENTS AND CORRELATION WITH PL DATA

Table III lists the nomalized PL intensity of n-InP substrates(N = 1x10 cm) at each individual fabrication step of the MIS structure. The PL intensity(arbitrary units) is around 1 for a InP surface cleaned by Br-MeOH etchant. Generally speaking, the PL intensity increases after immersing the InP sample into an aqueous acid solution and decreases after immersing a similar samlpe into an aqueous H O solution, in agreement with prior reports( ). Among all acids, the H SO solution results in the largest PL signal. Surface roughness created by chemical etches has been examined by optical scatterometer at the university of New Mexico (Dr. JR. Mcneil) and we found no correlation to the PL intensity trend.

Therefore, we can exclude the consideration of light scattering by chemically induced surface roughness.

Resistivity of the LCVD AlN films measured at a electric field strength of 2 MV/cm, is determined by a steady state current versus time measurement to be about 10 ohm-cm (AlN bulk value 10 ohm-cm). Breakdown field strengths for LCVD AlN films are in the range from 2 to 4 MV/cm. The leakage current and resistivity of LCVD films deposited at the same substrate temperature are independent of predeposition surface cleanings. However, the electrical properties of the AlN/InP interface depend markedly on the predeposition chemical surface cleaning. Figs. 3(a) and (b) show high frequency (1 MHz) C-V characteristics for two of the MIS structures both deposited at 300 C on n-InP. One is cleaned with NRL solution prior to AlN deposition and one is cleaned with H_2O. Note that a qualitative correlation is observed between the observed PL intensity following the substrate clean and the interface state density N_{ss} as determined by MIS C-V data. The sample with H_2SO_4 solution cleaning has similar C-V characteristics (shown in Fig. 4) to the sample with NRL cleaning. Both also have the same PL intensity following surface cleaning. The sample subject to H_2O cleaning has a distinct C-V characteristic (large N_{ss}) which corresponds to the smaller observed PL intensity.

A measured capacitance versus bias voltage curve measured at 1 MHz for AlN films in the MIS structure is shown in Fig. 4. The InP substrate was etched with a $4H_2SO_4 : 1H_2O_2 : 1H_2O$ solution prior to the LCVD AlN deposition. The measured hysteresis is small, even when the bias ramp voltage was 10 volts. An accurate knowledge of the substrate doping

density is required for calculation of the ideal C-V curve. Meiners( ) pointed out that the doping density of a wide band gap semiconductor(e.g. InP, GaAs) as measured from the deep-depletion method is more accurate than those obtained from Hall measurements. Using the deep-depletion method, we measured the carrier density to be 2.3x10 cm . From the measured substrate doping density and measured value of dielectric capacitance obtained from accumulation, a theoretical capacitance curve neglecting the effect of surface states was calculated. This ideal C-V plot is given in Fig. 4 as the dotted line. The agreement between the theoretical minimum value of capacitance and the measured capacitance data suggests that the InP surface under the AlN insulator can reach inversion, i.e. a p-channel can be formed in the n-type InP substrate. Using the Terman method( ), an analysis of the results shown in Fig. 5 indicates that a minimum surface states density occurs and is equal to about 3x10 eV cm and is located 0.4 eV below the conduction band edge.

Frequency dispersion characteristics as shown in Fig. 6, have been measured from 10 KHz to 2 MHz for both AlN/Si and AlN/InP samples. The accumulation capacitance increases monotonically with decreasing frequency from 10 KHz to 2 MHz. The observed behavior is in agreement with Ahrenkiel et al( ). and Sawada et al( ). but not with Meiners( ). In the accumulation region, both Si and InP substrates with AlN MIS structures showed that the curves disperse less than 10% in that frequency region. But in the depletion region, the frequency dispersion characteristics of MIS structures are quite different for the Si and InP substrates. The AlN/InP sample displayed a very large dispersion while the AlN/Si substrate was

stable. In general both the semiconductor/insulator surface state density and the bulk properties of the insulator could cause the frequency dispersion. The frequency dispersion in the accumulation region is attributed to the traps in the insulator bulk. But the frequency dispersion in the depletion region is attributed primarily to the surface state density. Clearly, there is a higher surface state density for the InP sample than for the Si sample due to the very different native oxide layer.

V. CONCLUSION

In this work, AES analysis shows that the laser CVD technique can deposit stoichiometric 1:1 AlN films at low substrate temperature. The lower refractive index and resistivity observed for LCVD films arises due to both a lower film density and the small amount oxygen incorporated in the films. Inadvertent oxygen sources include the background vacuum chamber leakage, residual water contamination on sample surface and water contamination in the ammonia source. Our results indicate that the wet chemical predeposition wafer cleans influence strongly the electronic properties of InP surface and the associated MIS structure. Photoluminescence(PL) provides a useful guide to the effects of cleaning on surface properties. The wet clean of the n-type InP with an acid solution (HF, NRL and H_2SO_4 solution) gives high PL intensity, in contrast to the use of basic solutions (H_2O_2) which give lower PL signal. The surface conditions associated with different chemical wafer cleans were also verified by XPS analysis. Using H_2SO_4 solution for surface cleaning of InP substrate, we achieve a better C-V curve for the AlN MIS structure.

Agreement between the calculated and the measured minimum capacitance values in our C-V curves suggest that a strong inversion layer was formed in the n-InP, surface etched with the H SO solution prior LCVD of AlN as the gate dielectric. The measured resistivity of LCVD AlN is about 10 ohm-cm at a applied field of 2 MV/cm and the breakdown voltage is about 2 to 4 MV/cm. By using the Terman method, we determined the surface state density distribution which turns out to have a minimum about 3x10 eV cm located 0.4 eV below the conduction band, comparable to other researchers' reports( ). LCVD deposited AlN films exhibit less than 10% dielectric frequency dispersion in 10 KHz to 2 MHz frequency range. The larger frequency dispersion of AlN/InP in the depletion region is judged to be caused by the existence of more surface states at the insulator/semiconductor interface.

ACKNOWLEDGEMENTS

The authors would like to thank the National Science Foundation, DARPA, and the Office of Naval Research for their support of this study.

Appendix B

preprint
11/3/87

Laser Induced Homoepitaxy of GaP

R. Solanki, U. Sudarsan,* and J. C. Johnson

Department of Applied Physics and Electrical Engineering

Oregon Graduate Center

19600 N.W. Von Neumann Drive

Beaverton, OR 97006-1999

Abstract

Laser induced pyrolytic process is utilized to 'direct-write' epitaxial GaP structures. The precursors used were trimethyl gallium and tertiarybutyl phosphine, a new phosphorous donor. Dependence of the epitaxial growth on several deposition parameters is examined.

*Department of Materials Science and Engineering

Laser-induced reactions have been successfully used for deposition of a wide range of materials [1]. An important attribute of this process is the high spatial resolution deposition that can be achieved without the use of photolithography. We describe below the application of this technique for epitaxial growth of GaP microstructures for potential optoelectronic applications.

Recently, several groups have reported deposition of epitaxial III-V compound semiconductors using either laser induced photolytic [2,3] or pyrolytic [4-7] reactions. These reactions are characterized by the laser wavelength and the absorption spectra of the reactant gases and the substrates. The latter process was employed for this investigation where the heating of the substrates was confined over very small lateral dimensions. The objective of the investigation reported here was to examine some of the deposition parameters required for selective epitaxial growth of GaP.

The experimental configuration is sketched in Figure 1. The 514.5 nm output from an Argon ion laser first passes through a beam expander and then is steered into a multi-element f/5.6 focusing lens. The lens was mounted on a precision X-Y stage, which can be translated a maximum of 2 inches along each axis by stepper motors in increments of 0.1 μm. By programming the motions of the stepping motors it was possible to 'write' various geometric patterns. Typically 3 mm long lines and 500 x 500 μm pads were grown. A vidicon camera allowed us to visually monitor the location of the deposition and in-process growth. The substrates were placed in a stainless steel reaction cell which had a quartz window. The cell was designed to accommodate 2-inch diameter substrates. The gas manifold and the deposition cell were heated to about 120°C to avoid any condensation of the precursor gases, especially on the window. All the depositions reported below were obtained

under static gas conditions.

The precursor gases for deposition of GaP were electronic grade trimethyl gallium (TMG) and tertiarybutyl phosphine (TBP), which is a relatively new phosphorous source. TBP was selected over phosphine due to lower safety risks [8]. Once the cell was filled with appropriate partial pressures of the precursors, its pressure was brought up to one atmosphere with hydrogen. Several different substrates have been examined, however, the discussion here will be limited to GaP. Liquid encapsulated Czochralski (LEC) GaP substrates were used, which were first degreased in organic solvents, followed by a one minute etch in a 10:1:1 mixture of H_2SO_4:H_2O_2:H_2O. This was followed by a DI water rinse and dry blowing with nitrogen before they were loaded into the deposition cell.

One of the first series of experiments involved examination of the partial pressures of the precursor gases. As expected, the growth rates increased with partial pressures at constant laser conditions. For example, at TMG partial pressure of 12 torr, V/III ratio of 15 and laser power of 2W, GaP depositions over 2 microns thick were obtained with a single scan. These depositions were obtained on several different substrates, including Si and GaAs. However, these deposits proved to be polycrystalline. Obviously the growth rates had to be reduced in order to obtain epitaxial films. This was achieved by reducing the concentrations of the precursors and using low power, multiple laser scans.

Smooth and continuous epitaxial lines and pads (by raster scanning) were deposited over a range of scan speeds (50 - 125 μm) and laser power (1 to 2 W) at TMG partial pressures of 2 to 4 torr and V/III ratio range of 10 to 20. The growths were stoichiometric over this V/III ratio range. The thickness of the deposits as a function of the number of scans is shown in Figure 2, where

the scan speed was 100 μm/sec, V/III ratio of 10, and laser power of 1 W. It can be seen that initially the growth per scan is relatively high, however it gradually decreases. Simple calculations show that the concentration of the reactants was enough to write at least 10^3 more structures. Therefore, depletion of reactants was not considered to be the reason for leveling off of the growth/scan. We feel one of the reasons for the slowing of the growth is the decrease in laser intensity. This can be visualized by considering the projection of a circular area on the spine of a ridge structure. As the growth progresses, the height of the ridge increases which further increases the projected area on it. This in turn reduces the laser intensity. A simple model based on this premise agrees with the observed trend in growth/scan.

An example of a direct-write structure is shown in Figure 3, which is a scanning electron micrograph. End view of this structure measures about 6.3 μm wide at the base and 2.5 μm high. Gaussian curve fit to profilometer data showed reasonable agreement, especially for the bottom half of the deposit. Top half of the deposit is slightly wider than the gaussian profile. The areas under these profiles (calculated by the profilometer) were proportional to their heights. Therefore the amount of deposition is represented in terms of their heights. An exception to this was at high laser power where double peaks were observed [9].

The crystalline properties of the direct-write structures were too small to be examined with an X-ray diffractometer, therefore transmission electron microscopy (TEM) was utilized. Cross-sectional samples were prepared using the standard procedure which includes ion milling. Figure 4 shows a typical electron diffraction pattern of the laser deposited GaP, which verifies epitaxial growth. TEM micrographs have also provided interesting information about defects in the substrate and in the epigrowth [10]. For example, a

relatively large number of defects are seen in the far wings of the cross-sectional profile. This is probably due to low growth temperatures.

The stoichiometry of the deposition was first examined using EDX and then Auger electron spectroscopy. Since the phosphorous precursor was organometallic and is not well characterized, our main concern was incorporation of carbon in the deposit. Figure 5 shows a typical Auger spectrum (after 2.5 min. Ar sputter) of the laser deposited epitaxial GaP. It can be seen that the incorporation of carbon in the growth is negligible. In this case the Ga and P atomic concentrations were 51.7% and 48.3%, respectively.

Another important growth parameter was found to be the scan speed. Figure 6 shows the dependence of the growth at 3 different scan speeds. At 50 μm/sec, although the initial growth rate is high, the profile becomes rough and irregular after a large number of scans. As the scan speed was increased, the profiles became smoother. The data in Figure 6 were obtained at TMG pressure of 4 torr, V/III ratio of 10, and 1 W laser power. Under these conditions best profiles were obtained at a scan speed of 100 μm/sec. At higher speeds the lines grown are discontinuous.

Other parameters examined included the laser power and the substrate orientation. The epitaxial growth rate initially increases with the laser power and then drops. For example, at TMG partial pressure of 3 torr, V/III ratio 15, and scan speed 100 μm/sec, the growth/scan first increased with laser power, then stayed approximately even between 0.9 to 1.2 W range, and then started to drop again. At higher laser powers the cross-sectional profile has a dip in the middle. Substrate temperatures during the laser scan have been estimated [11]. However, the calculated values are not consistent with our experimental results, therefore we are in the process of modifying

this theory.

All the results reported above were obtained on (100) GaP orientation. Besides (100), (111) orientation was also examined. For the first few scans (< 10), the growth/scan of the two orientations is about the same. However, as the thickness of the deposit increased with the number of scans, the growth rate on (100) was higher than that on (111) orientation. For example, under the conditions of Figure 3 and a scan speed of 100 μm/sec, a corresponding thickness on (111) orientation was 2.4 μm after 60 scans.

In summary, laser induced growth of epitaxial GaP structures have been demonstrated using a new phosphorous precursor. Multiple laser scans are required to grow thick epitaxial deposits, where growth/scan gradually slows down. Work is in progress to determine several other aspects of this process such as heteroepitaxy.

The authors would like to thank M. Bozack for doing the Auger analysis. This work is supported by DARPA under contract number F 49620-86-K-0021.

References

1. D. Bauerle, Chemical Processing with Lasers (Springer-Verlag, New York, 1986).
2. F. M. Donnelly, M. Geva, J. Long, and R. F. Karlieck, Appl. Phys. Lett. 44, 10 (1984).
3. V. R. McCrary, V. M. Donnelly, D. Brasen, A. Applebaum, and R. C. Farrow, Mat. Res. Soc. Proc. 75, 223 (1987).
4. W. Roth, H. Beneking, A. Krings and H. Krautle, Microelectronics Journal 15, 26 (1984).
5. N. H. Karam, N. A. El-Masry, and S. M. Bediar, Appl. Phys. Lett. 49, 880 (1986).
6. S. M. Bedair, J. K. Whisnant, N. H. Karam, D. Griffis, N. A. El-Masry and H. H. Stadelmaier, J. of Crystal Growth 77, 229 (1986).
7. Y. Aoyagi, M. Kanazawa, A. Doi, S. Iwai, and S. Namba, J. Appl. Phys. 60, 3 131 (1986).
8. C. A. Larsen, C. H. Chen, M. Kitamura, G. B. Stringfellow, D. W. Brown, and A. J. Robertson, Appl. Phys. Lett. 48, 1531 (1986).
9. For example, see Ref. 1, pg. 97.
10. To be published.
11. J. E. Moody and R. H. Hendel, J. Appl. Phys. 53, 4364 (1982).

Figure Captions

Figure 1. Schematic diagram of the experimental arrangement.

Figure 2. Epitaxial growth versus the number of scans at 2, 3 and 4 torr TMG partial pressures.

Figure 3. Scanning electron micrograph of a laser deposited line. The marker at the left represents 1 μm scale.

Figure 4. Transmission electron diffraction pattern of the laser deposited GaP. The zone-axis is [110].

Figure 5. Auger spectrum of the laser deposited GaP.

Figure 6. Dependence of the epitaxial growth on the laser scan speed.

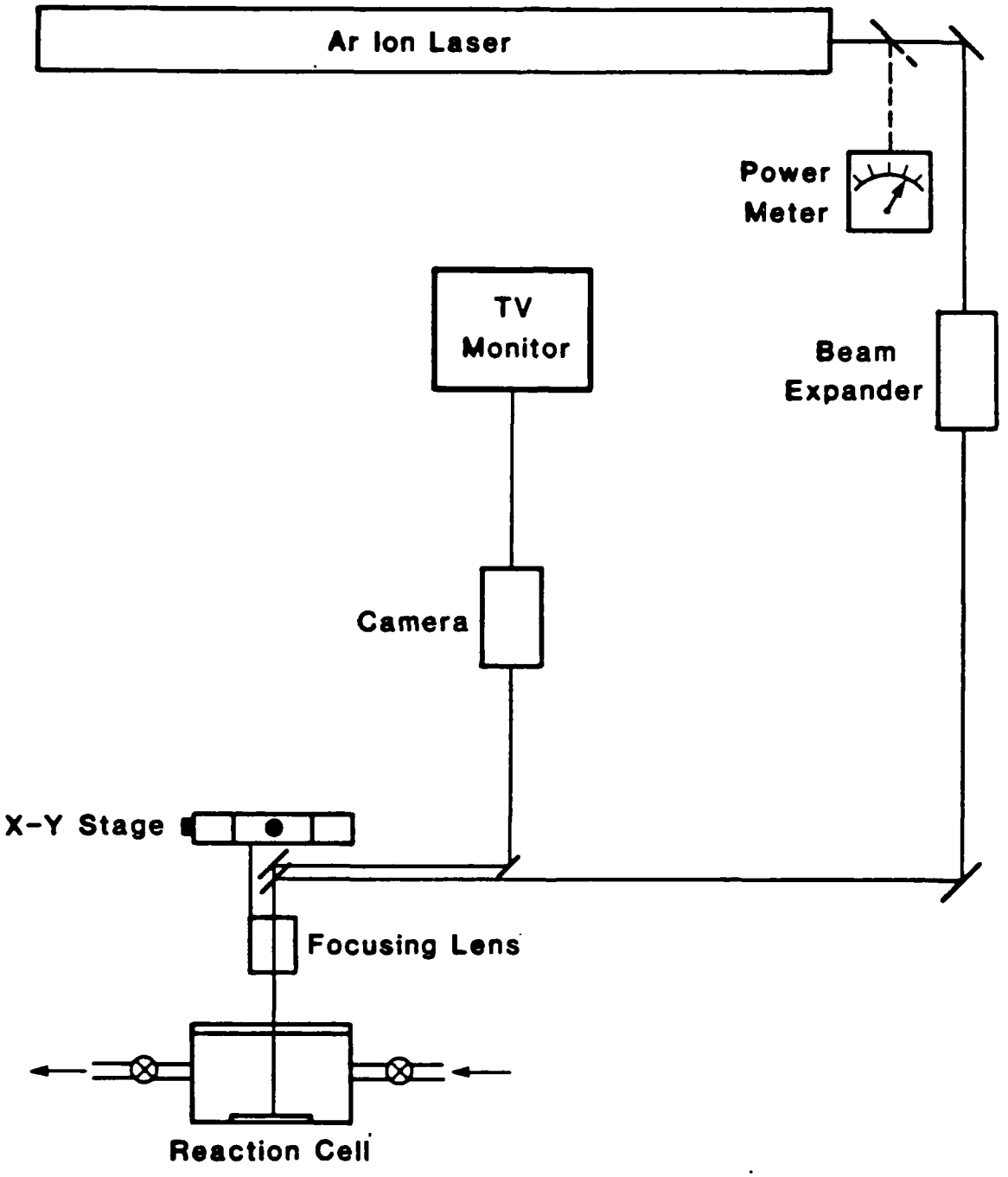
Ar Ion Laser
Power
Meter
TV
Monitor
Beam
Expander
Camera
X-Y Stage
Focusing Lens
Reaction Cell

FIG. I

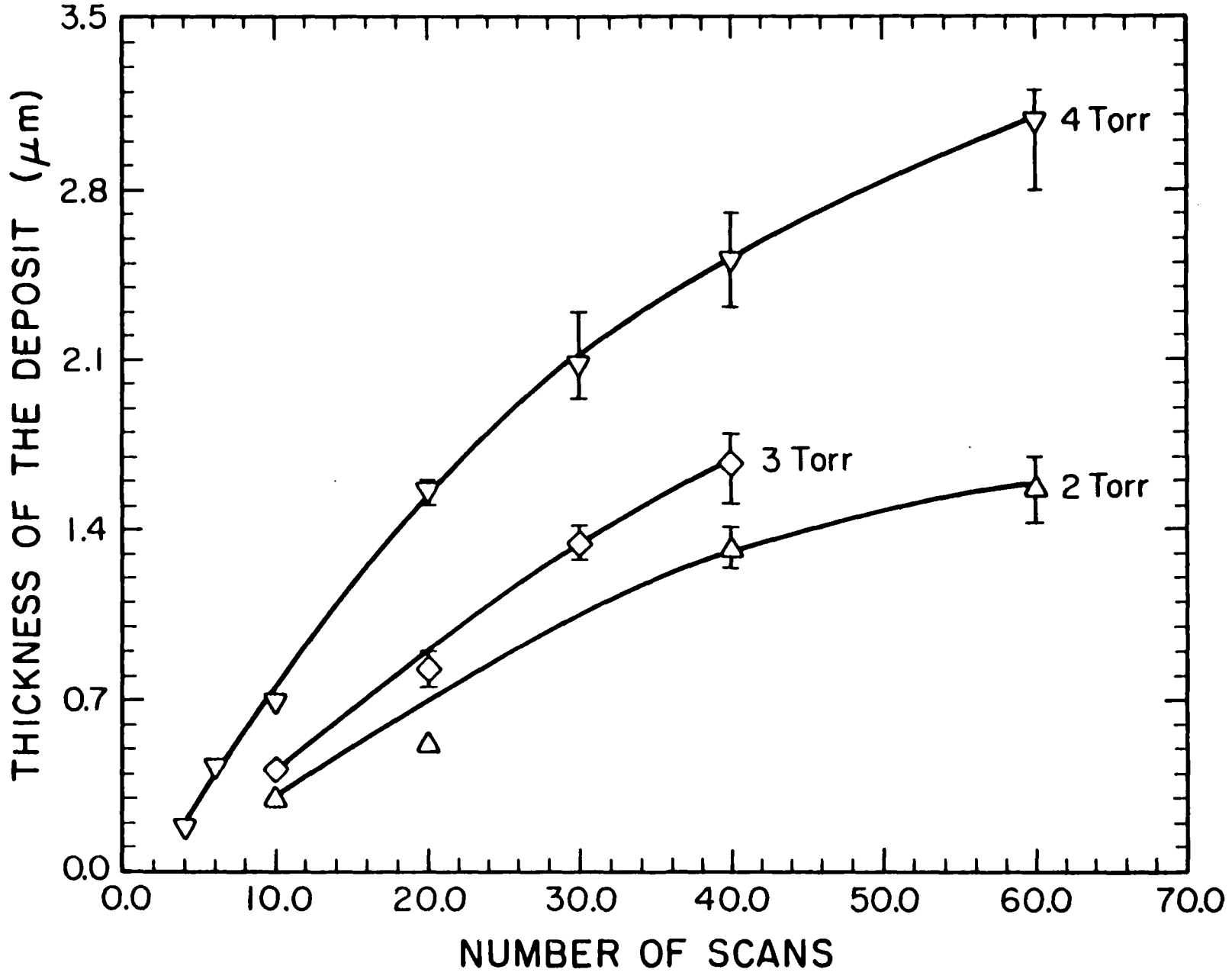
3.5
2.8
2.1
1.4
0.7
0.0
THICKNESS OF THE DEPOSIT (μm)
0.0
10.0
20.0
30.0
40.0
50.0
60.0
70.0
NUMBER OF SCANS
4 Torr
3 Torr
2 Torr

FIG. 2

FIG. 3

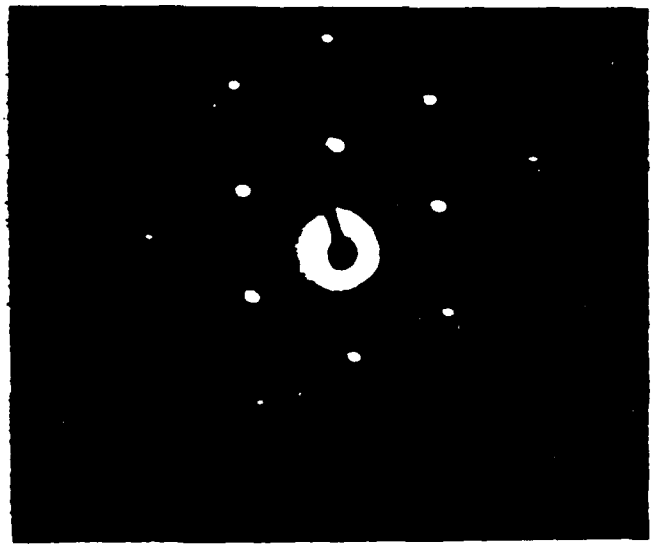

FIG. 4

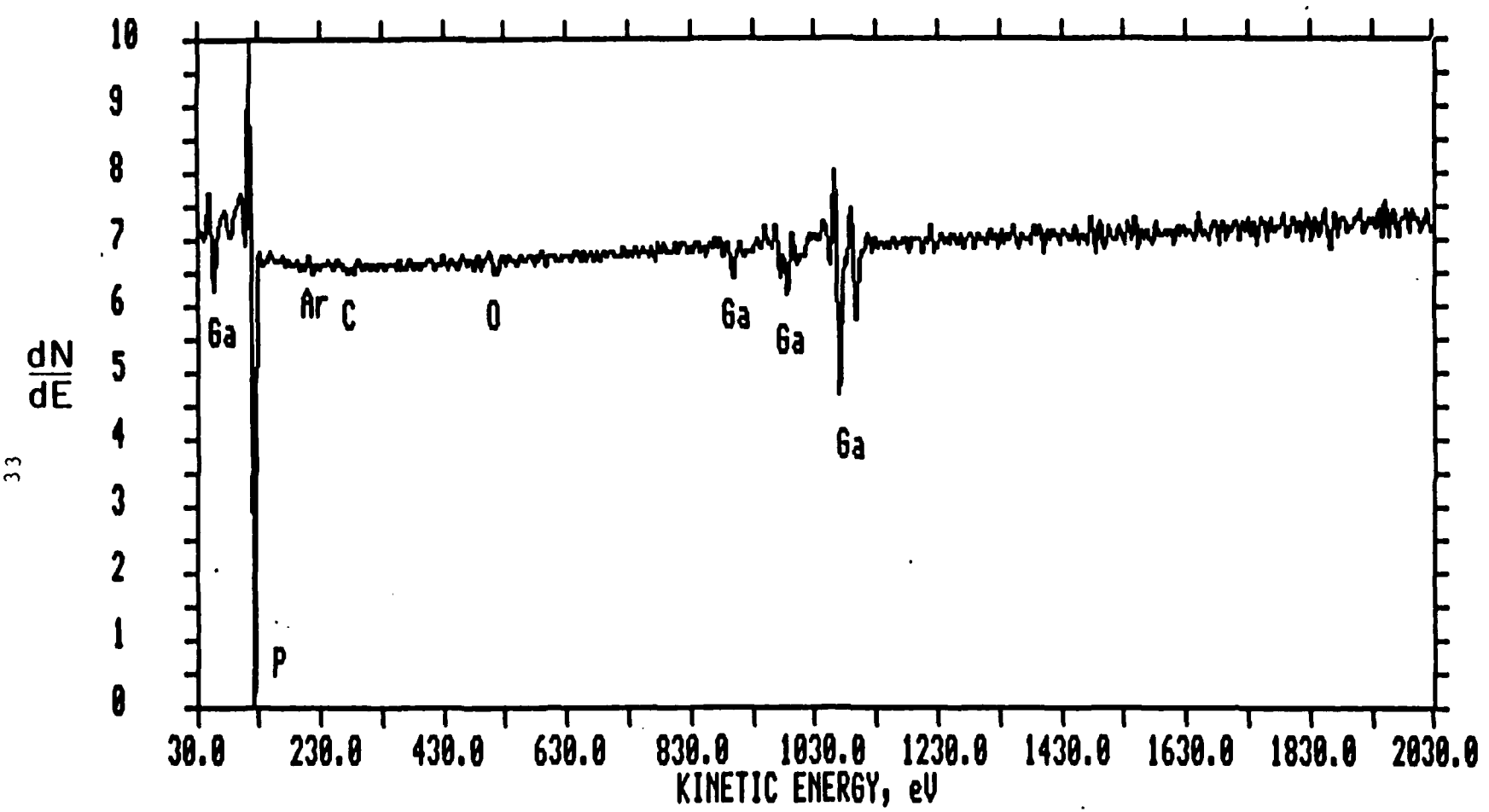
10
9
8
7
6
5
4
3
2
1
0
dN
dE
Ga
Ar
C
O
Ga
Ga
Ga
P
30.0
230.0
430.0
630.0
830.0
1030.0
1230.0
1430.0
1630.0
1830.0
2030.0
KINETIC ENERGY, eV

FIG. 5

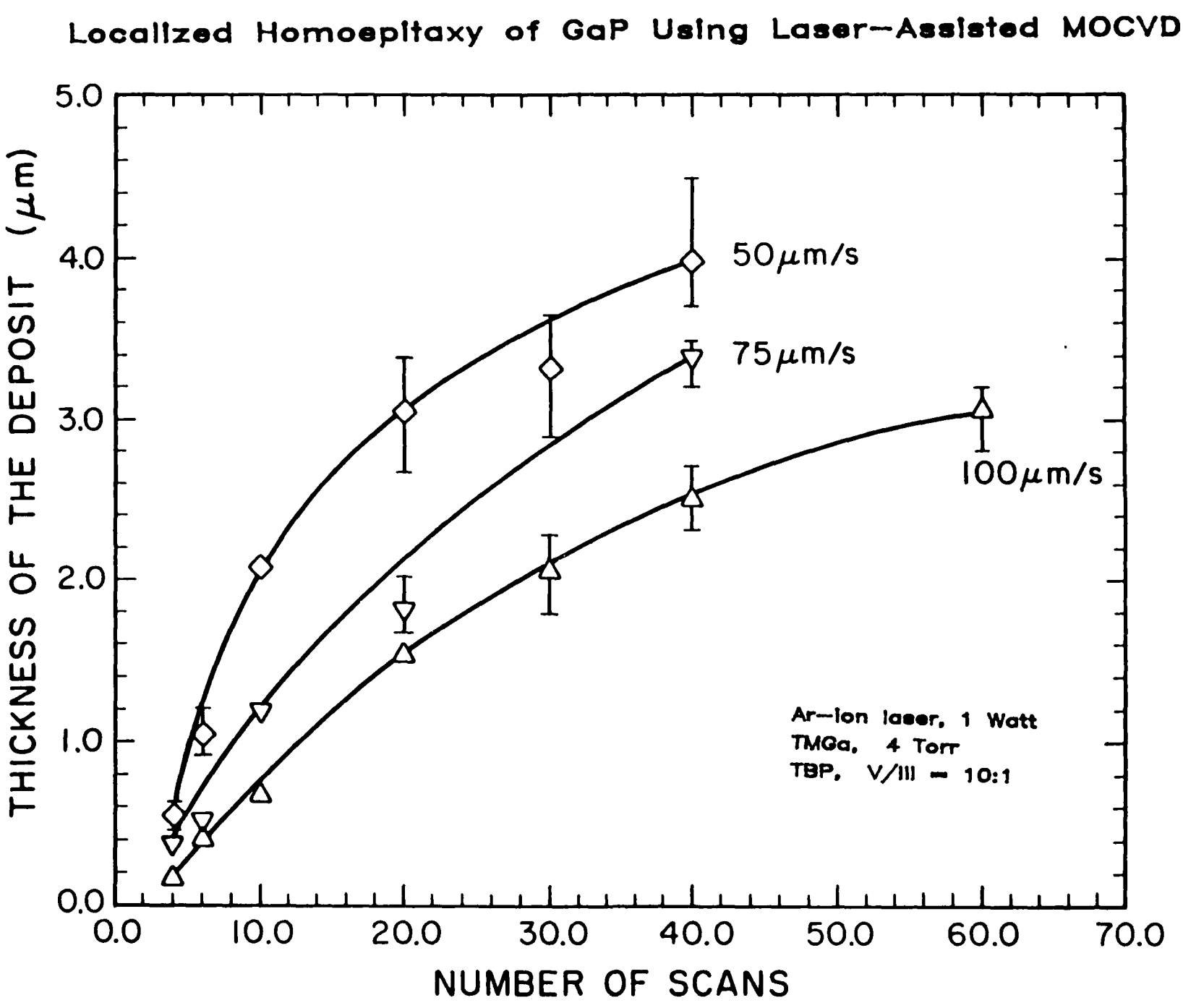
Localized Homoepitaxy of GaP Using Laser-Assisted MOCVD
THICKNESS OF THE DEPOSIT (μm)
NUMBER OF SCANS
5.0
4.0
3.0
2.0
1.0
0.0
0.0
10.0
20.0
30.0
40.0
50.0
60.0
70.0
50μm/s
75μm/s
100μm/s
Ar-ion laser, 1 Watt
TMGa, 4 Torr
TBP, V/III = 10:1

END

DATE

FILMED

4-88

DTIC